REPORT DOCUMENTATION PAGE

31Form Approved OMB No. 0704-0188

1. REPORT DATE *(DD-MM-YYYY)*	2. REPORT TYPE	3. DATES COVERED *(From – To)*
	Final Report	21 June 2004 - 21-Jun-05

4. TITLE AND SUBTITLE

A Detailed Study Of Polar Cap Ionospheric Dynamics By Multi-Instrument Techniques

5a. CONTRACT NUMBER
FA8655-04-1-3051

5b. GRANT NUMBER

5c. PROGRAM ELEMENT NUMBER

6. AUTHOR(S)

Professor j Moen

5d. PROJECT NUMBER

5d. TASK NUMBER

5e. WORK UNIT NUMBER

7. PERFORMING ORGANIZATION NAME(S) AND ADDRESS(ES)

University of Oslo
Box 1048 Blindern
N-0316 Oslo
Norway

8. PERFORMING ORGANIZATION REPORT NUMBER

N/A

9. SPONSORING/MONITORING AGENCY NAME(S) AND ADDRESS(ES)

EOARD
PSC 821 BOX 14
FPO 09421-0014

10. SPONSOR/MONITOR'S ACRONYM(S)

11. SPONSOR/MONITOR'S REPORT NUMBER(S)
Grant 04-3051

12. DISTRIBUTION/AVAILABILITY STATEMENT

Approved for public release; distribution is unlimited.

13. SUPPLEMENTARY NOTES

14. ABSTRACT

This report results from a contract tasking University of Oslo as follows: The Grantee will investigate ionospheric polar plasma patches using a detailed study of polar cap ionospheric dynamics using multi-instrument methods.

15. SUBJECT TERMS

EOARD, Magnetosphere, Space Weather, Ionosphere

16. SECURITY CLASSIFICATION OF:			17. LIMITATION OF ABSTRACT	18, NUMBER OF PAGES	19a. NAME OF RESPONSIBLE PERSON
a. REPORT	b. ABSTRACT	c. THIS PAGE			MICHAEL KJ MILLIGAN, Lt Col, USAF
UNCLAS	UNCLAS	UNCLAS	UL	31	19b. TELEPHONE NUMBER *(Include area code)* +44 (0)20 7514 4955

FINAL REPORT

on

A DETAILED STUDY OF POLAR CAP IONOSPHERIC DYNAMICS BY MULTI-INSTRUMENT TECHNIQUES

by

Professor Jøran Moen, PI

5 MAY, 2006

Correspondence to:
Prof. Jøran Moen
Department of Physics
P.O. Box 1048, Blindern
N-0316 Oslo, Norway
e-mail: jmoen@fys.uio.no

1. BACKGROUND INFORMATION

The EISCAT incoherent radar facilities consist of 3 radar systems. The UHF (933 MHz) and the VHF (224 MHz) located in northern Scandinavia, and the EISCAT Svalbard Radar (ESR) located in Longyearbyen, Svalbard. The UHF is the only three static incoherent scatter radar system in the world, with a transmitting and receiving antenna (32 m parabolic dish) located at Tromsø, and two additional receiving antennas in Sodankylä, Finland and Kiruna, Sweden. The Tromsø VHF system has a 5000 m^2 reflector with a meridional beam steering. The ESR is the last generation incoherent radar located within the polar cap. The system comprises two parabolic dish antennas sharing the same transmitter and receiver system, working at 500 MHz. ERS-1, is a 32-m diameter antenna, which can swing 540^0 in azimuth and from 0 to 180^0 in elevation. ERS-2, 42 m in diameter, is a fixed beam oriented along the magnetic field line. The ESR radar facility is located on the mountain of Mine 7, within 6 km from the Longyearbyen Auroral Station. With the three EISCAT radar systems working together it is possible to provide a spatial radar coverage of up to ~20^0 in magnetic latitude, with high time and spatial resolution.

The Ny-Ålesund (geogr. lat 78.9^0N; geomagnetic lat. 76.1^0 ILAT) and Longyearbyen Auroral observatories (geogr. lat 78.2^0N; geomagnetic lat. 75.3^0 ILAT) are the master stations in our Svalbard network. The main optical instruments are meridian scanning photometers (MSP) and All-Sky CCD imagers at different wavelengths.

The CUTLASS HF radar has complemented the EISCAT and optical ground-measurements with a 2-dimensional field of view above the Svalbard archipelago. The coherent scattered signals from the CUTLASS radar (part of SuperDARN) constitute a powerful tool for investigations of both temporal and spatial behaviour of the polar cap electrodynamics.

Whenever possible, our ground observations have also been correlated with in-situ measurements from low-altitude polar orbiting satellites (NOAA, DMSP, Polar and Cluster) as well as space platform observations of the solar wind (ACE).

2. SCIENTIFIC RESULTS

On this project we have published 3 papers of which the abstracts are listed in section 2.1-2.3. Section 2.4 reports yet unpublished results on a new category flow events in the cusp inflow region, Reversed Flow Events (RFEs). The term RFE refers to flow channels in which flow direction is opposite to the large-scale background convection.

2.1 Paper 1

Oksavik, K., J. Moen, and H. C. Carlson, High-resolution observations of the small-scale flow pattern associated with a poleward moving auroral form in the cusp, Geophys. Res. Lett., 31 (11), L11807, doi:10.1029/2004GL019838, 2004.

Abstract: In this paper we present high-resolution observations by the EISCAT Svalbard Radar of the localized ionospheric flow response due to one single flux transfer event and the

relative location of a poleward moving auroral form. In a fast scan mode the radar was tracking a 50–60 km wide channel of westward flow in the cusp region. This flow channel was surrounded by flow running in the opposite direction. At the poleward edge of the narrow flow channel a poleward moving auroral form was situated, consistent with the auroral form being the signature of an upward Birkeland current filament. Our observations can be interpreted in terms of the Southwood [1985, 1987] flux transfer model, and the FTE twin-cell flow pattern appears to be a ripple onto the larger-scale background convection.

2.2 Paper 2

Moen, J., K. Oksavik, and H. C. Carlson, On the relationship between ion upflow events and cusp auroral transients, Geophys. Res. Lett., 31 (11), L11808, doi:10.1029/2004GL020129, 2004.

Abstract: In this paper we present a one-to-one relationship between poleward moving auroral forms (PMAFs) in the cusp and ion upflows. Ion upflows have the same quasi-periodic nature as cusp auroral transients, which are believed to be a signature of flux-transfer events. This new observation corroborates the idea that low energy particle precipitation is the dominant source of energy for ion upflows. Some events were lacking elevated Ti which indicates that frictional heating is not required. The ion upflow events broadened with altitude in characteristic V-shape. We suggest that each PMAF was associated with an inverted V-potential structure moving over the radar.

2.3 Paper 3

Oksavik, K., J. Moen, H. C. Carlson, R. A. Greenwald, S. E. Milan, M. Lester, W. F. Denig, and R. J. Barnes, Multi-instrument mapping of the small-scale flow dynamics related to a cusp auroral transient, Ann. Geophys., 23 (7), 2657-2670, 2005.

Abstract: In this paper we focus on flux transfer events (FTEs) and poleward moving auroral forms (PMAFs) in the cusp region, combining data from the EISCAT Svalbard radar, SuperDARN HF radars, ground-based optics, and three low-altitude polar-orbiting spacecraft. During an interval of southward interplanetary magnetic field the EISCAT Svalbard radar tracked a train of narrow flow channels drifting into the polar cap. One 30–60 km wide flow channel surrounded by flow running in the opposite direction is studied in great detail from when it formed equatorward of the cusp aurora, near magnetic noon, until it left the field-of-view and disappeared into the polar cap. Satellite data shows that the flow channel was on open field lines. The flow pattern is consistent with field-aligned currents on the sides of the flow channel; with a downward current on the equatorward side, and an upward current on the poleward side. The poleward edge of the flow channel was coincident with a PMAF that separated from the background cusp aurora and drifted into the polar cap. A passage of the DMSP F13 spacecraft confirms that the FTE flow channel was still discernable over 15 minutes after it formed, as the spacecraft revealed a 30–40 km wide region of sunward flow within the anti-sunward background convection. From the dimensions of the flow channel we estimate that the magnetic flux contained in the event was at least 1 MWb. This data set also shows that Birkeland current filaments often seen by low-altitude

spacecraft in the cusp/mantle are really associated with individual FTE events or a train of FTEs in progress. As the region 0 or cusp/mantle current represents the statistical average consistent with the large-scale flow pattern, we therefore introduce a new term – FTE currents – to denote the unique pair of Birkeland current sheets that are associated with individual meso-scale FTE flow disturbances. The poleward moving auroral forms (PMAFs), often referred to in the literature, are the optical signature of the upward FTE current.

2.3 Reversed Flow Events observed by ESR

This section comprises a detailed report on a statistical study of flow transients observed near the cusp inflow region. It may be recommended to read **Summary section 2.3.6** first.

2.3.1 The data set

The data set examined consists of all ESR data collected from daytime runs of the fast azimuth scan mode with constant 30° elevation during 12 days between 16.01.2001-20.01.2001 and 15.12.2001-21.12.2001.

All data have been checked for signal drift and 3 scans from 17.01.2001 (6:01-6:02, 6:11-6:13 and 6:13-6:15 UT), 7 scans from 20.01.2001 (06:19 – 06:34 UT) and all data on 18.01.2001 were excluded from this study. 18 incomplete scans were also excluded. The remaining data set consists of 35 hours and 49 minutes of data in a total of 767 scans. Table 1 lists the dates (first column) and time intervals (second column) of available data and specific details about the scan pattern (column 3-7). The scans that are not used in the analysis are listed in column 8, and column 9 contains the total number of scans that went into the analysis for each time period. Column 10 lists the magnetic local time (MLT) difference in minutes between the MLT of the mid-position of each radar scan and the MLT of the radar site in Longyerbyen.

Since the ESR scans are at 30° elevation, the data is obtained from increasing altitude for increasing distance from the radar site. In order to ease the comparison with data from other sources there is a need to project the data along the magnetic field line to a common reference altitude of 250 km. Figure 1 shows demonstrates a sequence of line-of-sight velocity (v_i) van-plots for 16 December 2001. For the ion velocity, positive velocities (red) are directed away from the radar, whereas negative velocities towards the radar are coloured blue. Missing or bad data values are plotted as white. The date (day-month-year), scan time (HH:MM:SS - HH:MM:SS), and the scan rotation (ccw, counter-clockwise or cw, clockwise) is given in the title of each frame. Every counter-clockwise scan is further marked by a red astrix located at the ESR position in Longyearbyen.

2.3.2 Selection criteria

In general, the ion velocity data contains a lot of fine-structure. In this thesis, transient small-scale flow channels are of main interest. An example of such a feature is shown in Figure 1 encircled by a yellow ellipse. To distinguish these flow channels from other features in the data, several clear selection criteria had to be defined.

RFE-Reversed Flow Event definition: An event, or flow channel, is an elongated segment of enhanced ion flow in the opposite direction of the background flow. The background flow

is the large-scale plasma convection in the polar cap. SuperDARN convection maps were retrieved from JHU/APL and used to verify that the background flow in the radar field-of-view corresponds to the large-scale plasma convection.

Table 1 : Times with available radar data and specification of the scan modes used

Date (2001)	*Radar data available*	*Elevation [°]*	*Azimuth [°]*	*Scan width (azimuth) [°]*	*Period [sec]*	*Speed [°/sec]*	*Removed scans*	*# of scans in period*	*MLT Diff. [min]*
16.01.	*06:03:10-7:38:34*	*30*	*-75 to 15*	*90*	*128*	*0.703*	*None*	*45*	*-30*
16.01.	*08:34:22-11:01:34*	*30*	*-165 to -75*	*90*	*128*	*0.703*	*9:10, 9:20, 11:01*	*64*	*-70*
17.01.	*06:01:02-07:15:07*	*30*	*15 to 105*	*90*	*128*	*0.703*	*6:01, 6:11, 6:13,*	*32*	*+70*
17.01.	*09:16:02-10:50:38*	*30*	*-75 to 15*	*90*	*128*	*0.703*	*9:16,*	*44*	*-30*
18.01.	*06:05:07-07:34:18*	*30*	*30 to 90*	*60*	*192*	*0.313*	*all*	*0*	
19.01.	*06:02:38-07:57:47*	*30*	*15 to 105*	*90*	*128*	*0.703*	*None*	*54*	*+70*
19.01.	*09:31:42-11:59:46*	*30*	*-75 to 15*	*90*	*128*	*0.703*	*11:58*	*69*	*-30*
20.01.	*06:03:02-07:17:17*	*30*	*15 to 105*	*90*	*128*	*0.703*	*6:19-6:34 (7scans)*	*28*	*+70*
20.01.	*09:55:22-10:59:54*	*30*	*-75 to 15*	*90*	*128*	*0.703*	*10:59*	*30*	*-30*
15.12.	*06:03:54-07:46:15*	*30*	*0 to 120*	*120*	*192*	*0.625*	*6:38,7:01,*	*26*	*+70*
15.12.	*09:08:17-09:27:26*	*30*	*0 to 120*	*120*	*192*	*0.625*	*None*	*6*	*+70*
15.12.	*09:28:30-10:59:54*	*150 (30)*	*0 to 120 (180-300)*	*120*	*192*	*0.625*	*None*	*29*	*-70*
16.12.	*06:05:01-06:30:05*	*30*	*-60 to 60*	*120*	*192*	*0.625*	*None*	*8*	*-70*
16.12.	*06:30:43-08:19:28*	*30*	*0 to 120*	*120*	*192*	*0.625*	*None*	*34*	*+70*
16.12.	*08:20:06-09:30:24*	*30*	*-60 to 60*	*120*	*192*	*0.625*	*None*	*22*	*0*
16.12.	*09:31:28-10:59:54*	*150 (30)*	*0 to 120 (180-300)*	*120*	*192*	*0.625*	*None*	*28*	*-70*
17.12.	*06:05:30-06:58:27*	*30*	*0 to 120*	*120*	*192*	*0.625*	*6:30, 6:52, 6:56*	*9*	*+70*
17.12.	*10:01:01-10:59:44*	*150 (30)*	*0 to 120 (180-300)*	*120*	*192*	*0.625*	*10:58*	*19*	*-70*
18.12.	*06:31:02-08:06:59*	*30*	*0 to 120*	*120*	*192*	*0.625*	*8:03*	*29*	*+70*
18.12.	*09:22:59-10:31:47*	*150 (30)*	*0 to 120 (180-300)*	*120*	*192*	*0.625*	*10:30*	*21*	*-70*
18.12.	*10:45:10-10:59:54*	*30*	*-225 to 135*	*360*	*512*	*0.703*	*None*	*2*	*0*
19.12.	*06:00:51-08:20:26*	*30*	*0 to 120*	*120*	*192*	*0.625*	*8.08, 8:17*	*41*	*+70*
19.12.	*08:22:11-08:47:38*	*150 (30)*	*0 to 120 (180-300)*	*120*	*192*	*0.625*	*None*	*8*	*-70*
20.12.	*06:00:01-07:58:22*	*30*	*0 to 120*	*120*	*192*	*0.625*	*7:37*	*33*	*+70*
20.12.	*10:06:47-10:57:56*	*150 (30)*	*0 to 120 (180-300)*	*120*	*192*	*0.625*	*None*	*16*	*-70*
21.12.	*06:00:38-10:59:15*	*30*	*-180 to 180*	*360*	*256*	*1.406*	*None*	*70*	*0*

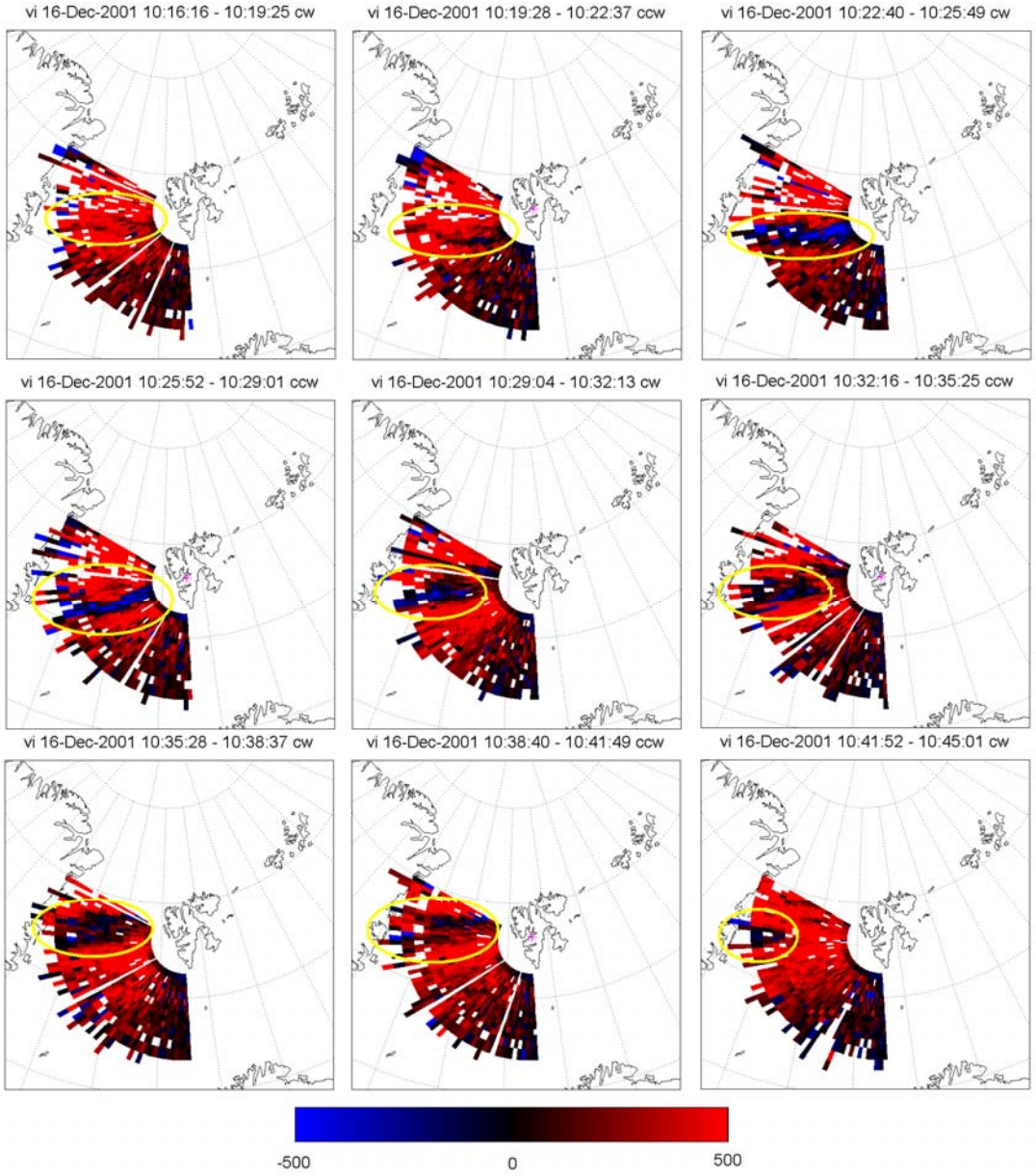

Figure 1: Typical ion velocity fan plot with data projected to 250 km. Positive velocities indicate ion flow directed away from radar. The RFE is encircled by a yellow ellips.

In order for an event to qualify as RFE the following set of criteria has to be fulfilled:

i. The RFE has to be evident in more than one radar beam direction/azimuth (this criterion should avoid bad measurements).
ii. The line-of-sight ion velocity inside the RFE must be greater than |250| m/s for at least one scan.
iii. The RFE has to have a longitudinally extent of at least 400-600 km in the radar field–of-view.
iv. The RFE has to stay in clear contrast to the background, i.e. the background flow must exhibit uniform velocities higher than |250| m/s in the area surrounding the RFE.

v. The RFE has to be embedded within the background flow for at least one scan (this criterion avoids that large-scale convection reversals are detected as RFE).

In many cases, RFEs start out as short and thin channels where the ion velocity is reduced compared to the background flow. This is shown in Figure 1 from 10:16-10:22 UT. Their velocity enhances then in the direction opposite to the background flow and they expand in width and length (seen from 10:22-10:29 UT). Eventually, but not generally, they broaden and/or move north/south before they fade out. The event in Figure 1 exhibits this behaviour from 10:29 to 10:45 UT.
A number of cases have been found where a region of the background flow has reversed or diminished, as in Figure 1 at 10:16-10:22 UT, but for some reason no further development to a RFE took place. These signatures in the ion velocity resemble events in the initial stage and are therefore defined as flow structures.

Flow Structure definition:
Flow structures are the same as RFE besides from:

i. The background flow field around a velocity feature can be more irregular/speckled and have velocities lower than 250 m/s (see Figure 2 *a*)
ii. The ion velocity structures represent a clear reduction the background flow (Figure 2 *b*)
iii. Speckled data, a high amount of white missing data points or the limitation of the field-of-view may make it difficult to decide whether a channel is a full event or a flow structure. In any case of doubt, the channel was rated as flow structure rather than RFE.

Figure 2 illustrates several flow structures that failed to qualify as RFEs. In Figure 2a the background is speckled and does not exhibit a clear velocity pattern. In Figure 2 *b* the structure is located on a uniform background of high velocity, and the ion velocity inside the structure is a clear reduction of the background flow, but its ion flow speed is not higher than 250 m/s. The flow structure in Figure 2 *c* is located on a uniform high velocity background and has a core with high, reversed velocity with respect to the background, but not enough of the flow structure is visible within the field-of-view in order to determine if it is long enough to fulfil the size requirements of the RFE definition. In Figure 2 *d* the small reversed flow signature near the north-eastern edge of the field-of-view does not have the longitudinal extent to qualify as RFE. In Figure 2 *e* and Figure 2 *f*, the flow structure has sufficient velocity and is located on a uniform high velocity background, but as in Figure 2 *c* too little of the flow structure is visible to be qualified as a RFE. In addition, the high amount of missing data points in Figure 2 *f* makes it impossible to know whether the velocity inside the flow structure is sufficiently high.

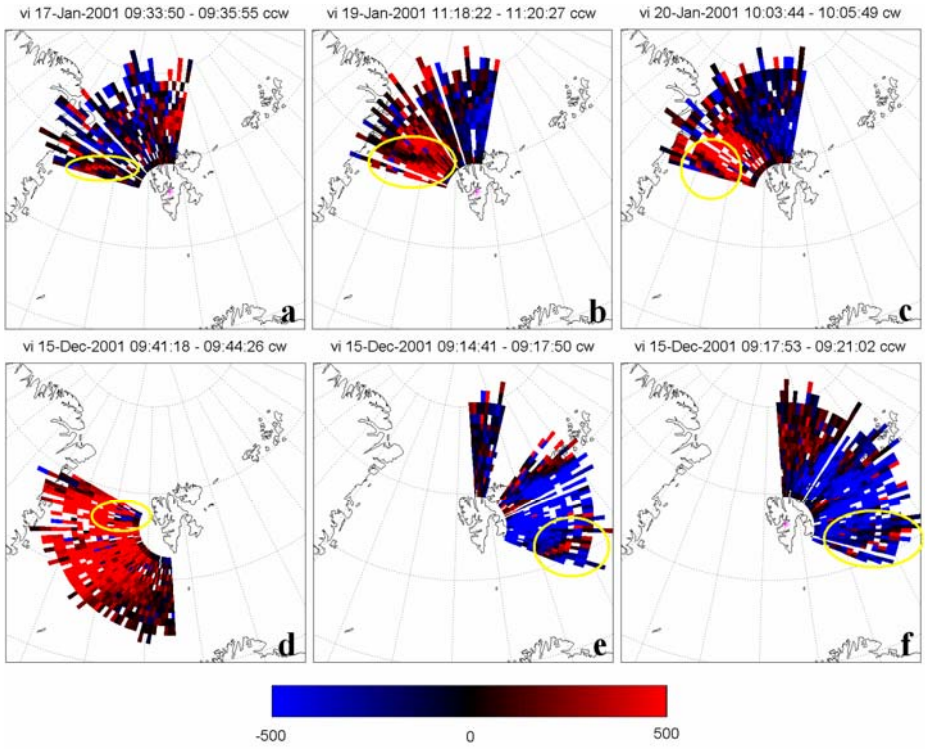

Figure 2: Different types of flow structures that do not fulfil all criteria required to classify it as a reversed flow event (RFE): a) speckled background with no clear velocity higher than 250 m/s in either direction, b) clear reduction of the background flow but insufficient to reverse the flow, c) flow structure is partly outside the field-of-view, d) flow structure is too short in longitude, e) structure is terminated by the radar field-of-view, and f) too much speckle/missing data points.

2.3.3 Data survey

Table 2 lists the RFEs and flow structures identified in the data set together with attributes for further analysis which are described below:

N°: Indicates the number of occurrences of a given event or structure. Events and structures are numbered separately.

Class: Describes whether a given signature meets the criteria of a RFE (marked E) or a flow structure (marked S). Flow structures and their attributes are coloured green for easier distinction.

Date: Lists the date when a given event or structure occurred.

Start/Stop: These columns lists the start/stop times of the first/last scan when an event was visible. The very first and last signs which could be associated with an RFE or flow structure have been taken as beginning and end times.

 # scans: States the number of consecutive scans where a signature is visible.

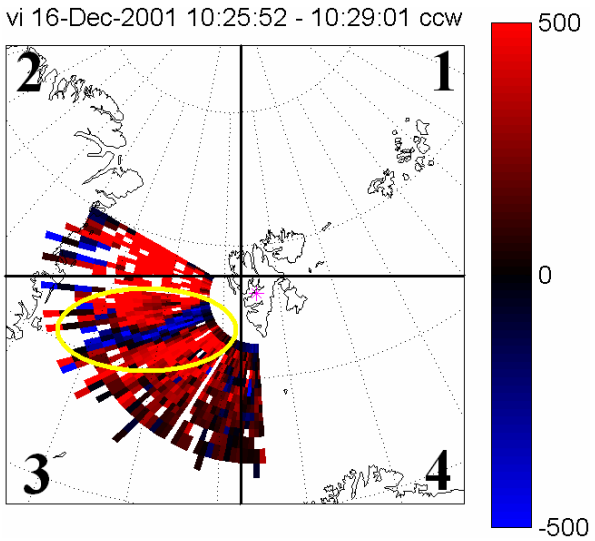

Figure 3: Definition of quadrants used to sort the RFEs and flow structures in *Error! Reference source not found.*. ***In the example shown the RFE, seen as a blue stripe inside the yellow ellipse, is located in the third quadrant.***

Period [s]: The time interval it takes to perform one complete radar scan inferred from Table 1.

Dur. [s] (Duration): Gives the lifetime in scans of one single RFE/flow structure.

Q (Quadrant): Indicates in which of the four quadrants defined in Figure 3 an event or structure is located. The RFE in Figure 3, visible as blue stripe inside the yellow ellipse, is located in the third quadrant.

F.dir. (Flow direction): This column gives the direction of the ion flow of the RFE or flow structure with respect to the geographic coordinate system. Flows are abbreviated as follows: Northeast (N/E), Northwest (N/W), Southeast (S/E), Southwest (S/W). The direction of the blue RFE in Figure 3 is towards northeast (N/E).

abs(V_i): The absolute value of the ion velocity of the flow event or flow structure, given within ranges of 0 - 250, 250 – 500 m/s or larger.

M (Motion): Indicates whether or not the RFE or flow signature propagates north (N) or south (S).

W (Widening): Indicates whether a RFE or flow signature widens throughout its lifetime, indicated by an "x".

Backg. (Background): Indicates whether the background flow is "red" (high velocities directed away from the radar with v_i > 250 m/s), "blue" (high velocities directed towards the radar with v_i < -250 m/s), or "black"/speckled (with velocities between -250 and +250 m/s).

F.o.v. (Field-of-view): An "x" is set in this column whenever a signature is determined by a change in the radar field-of-view, or where the onset not necessarily was seen due to a change of the scan mode. "Poor data" indicates that a RFE or structure has been determined by using unreliable data.

IMF B_z: States the time shifted polarity of the IMF B_z component during an event (see Chapter 4). Terms used are "> 0", "< 0" or "fluct" for "fluctuates" if the polarity changes sign and fluctuates during the event.

IMF B_y: Similar to IMF B_z above.

Certainty: Indicates by using letters how reliable the IMF polarity for B_z and B_y is, after uncertainty in the time delay is taken into consideration for the time delay estimate. If the delay calculated from the Brute Force method and the delay inferred from the Lockwood method gives exactly the same polarity the letter "A" is used. "*B*" is used if the polarity is most likely correct but there were small changes in IMF, and "*C*" if it is very uncertain or the brute force and Lockwood methods leads to different results for the polarity. The first letter is assigned to IMF B_z, the second for IMF B_y. Hence, "*AA*" means that both the IMF B_z and B_y polarities are not expected to be affiliated with any uncertainty, whereas "*AC*" for instance means that the IMF B_z polarity is expected to be correct, but the IMF B_y polarity is associated with uncertainty with respect to the timing of a polarity change.

SD coverage: This column indicates whether SuperDARN had data coverage at the location of the ESR fan shaped field-of-view at any time. "No data" means that there are no flow vectors at the location of the ESR fan, and convection is calculated entirely by the SuperDARN model [Ruohoniemi and Baker, 1998].

SD match: This column indicates how well the large-scale convection calculated by SuperDARN matches the background flow seen in the ESR field-of-view for every scan. If there was no data at the location of the scan, no match is indicated.

Along/opposite F_t: Indicates whether or not the flow of a flow event or a flow structure is directed along with or opposite to the direction in which the magnetic tension force pulls newly opened field lines after reconnection for a given IMF B_y polarity. In the case of a velocity reduction, it was assumed that the flow was opposite to the background flow.

Example: Event 10, 16.12.2001

The event shown in Figure 1, listed as number 10 in Table 2, is used as an example to explain Table 2. An enlarged SuperDARN convection map indicating the ESR field-of-view is shown in Figure 5, and the whole SuperDARN sequence covering the time period of the RFE is shown in Figure 7. SuperDARN has good coverage at the location of the ESR field-of-view except from the map at 10:40 UT. Svalbard is located slightly post-noon in a region of high plasma convection directed mostly westwards. This convection pattern is consistent with the background flow seen from the ESR which saw flow

directed away from the radar (westwards) except from the southern part of the scan where the ESR line-of-sight velocity is not sensitive to zonal flow. Hence, the scans from 10:22 to 10:35 UT on 16.12.2001 fulfil all the requirements of a RFE and it is therefore marked E in the second column of Table 2*a*. The first sign of a velocity reduction compared to the background is visible at 10:16 UT, and the RFE is not visible after 10:45 UT. The RFE lasts over 9 scans. From Table 1 each scan was 128 s, and the total duration for the nine scans was 1728 s. The RFE is located in the third quadrant, as can be seen from Figure 3, and the ion flow is directed towards northeast (N/E). The ion velocity inside the event reaches an absolute velocity of 250-500 m/s or more, and it moves north and widens with time. The background flow is clearly "red" (250-500 m/s directed away from the radar), and the RFE is not determined by a change in the radar field-of-view (hence, no "x" is set in that column). From the IMF plots in Figure 3, both the IMF B_z and B_y polarities where determined to be clearly "> 0" (sixth and seventh column of Table 2b). The difference between the delay inferred from the Brute Force and the Lockwood method was ~10 minutes (see Figure.4), and "*AA*" indicates a high certainty for both polarities even taking the different delays into account. For a positive IMF B_y, the magnetic tension force would pull newly opened field lines westward, and there should plasma flow in the same direction. The ion flow event is however directed towards the northeast, so it is opposite to the direction of the magnetic tension force.

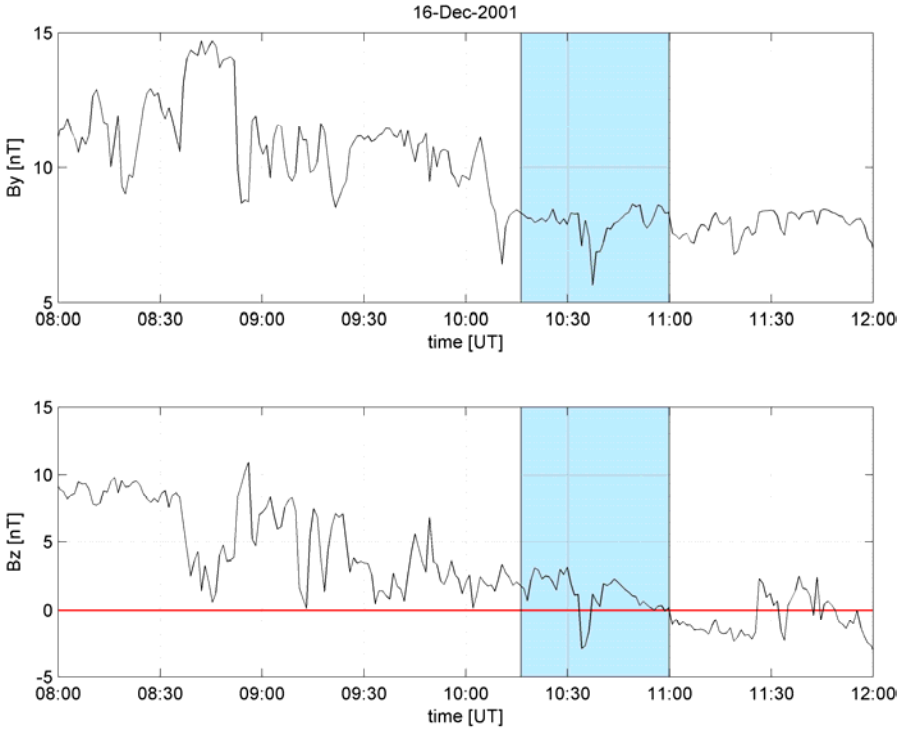

Figure 3: The IMF B_y and B_z components as measured by the ACE spacecraft, time shifted by 47 min as calculated from the Brute Force method. The time shown is thus time$_{ACE}$ + 47 min. The blue shaded areas indicate the time interval of RFE 10 and 11.

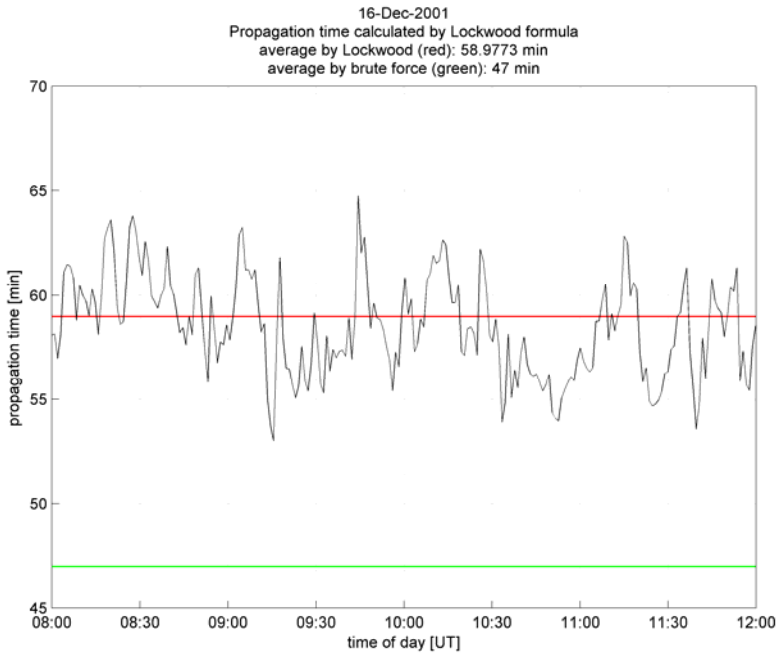

Figure.4: The time delay calculated by the Lockwood method. The red line indicates the average time delay from the Lockwood method, the green line indicates the average time delay calculated from the Brute Force method.

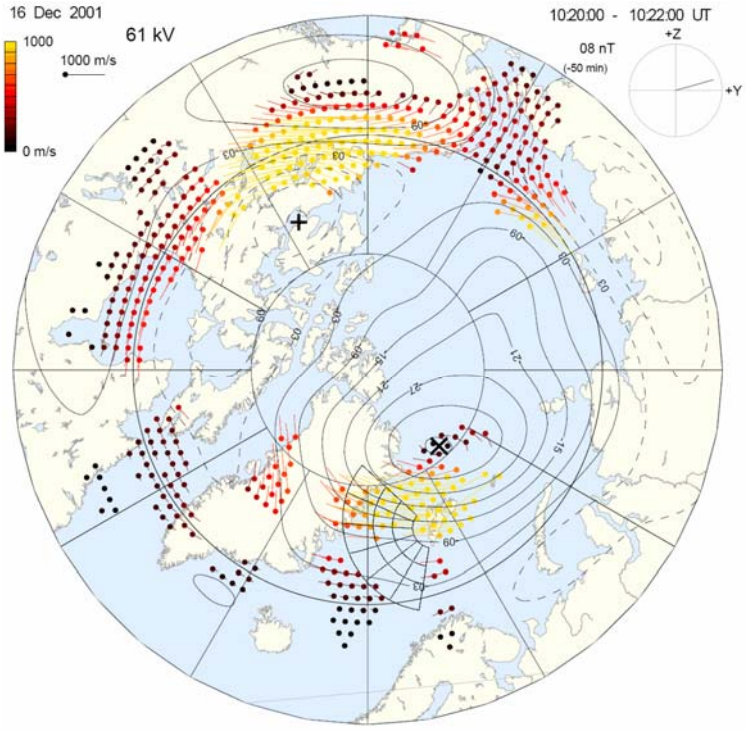

Figure 5: Enlarged map of the SuperDARN global convection pattern. Indicated are polar cap potential contours of the SuperDARN map-potential model and flow vectors based on SuperDARN measurements of the convection. Noon (12 MLT) is at the bottom. In addition, the ESR field-of-view has been superimposed onto the figure).

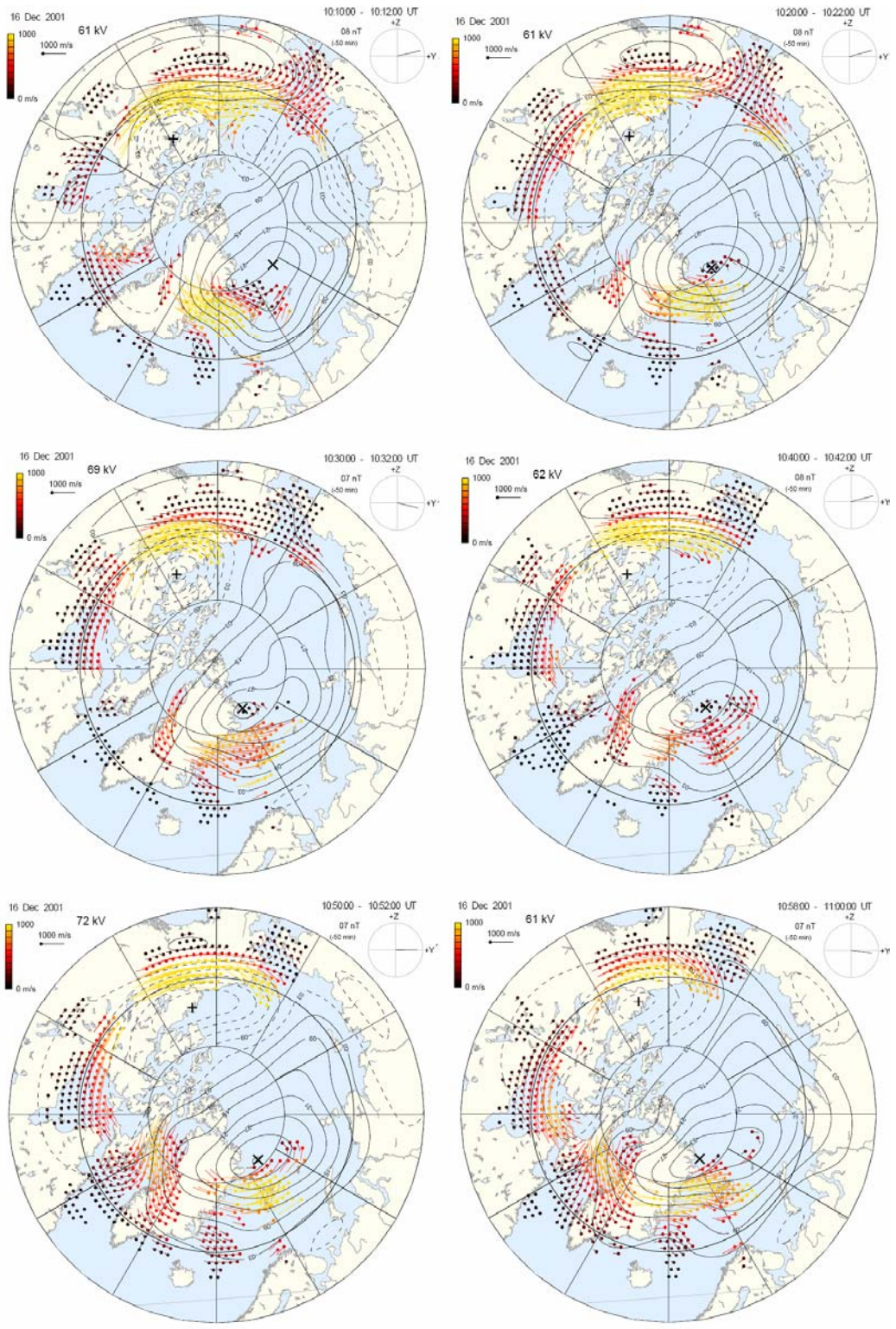

Figure 6: A sequence of SuperDARN global convection patterns. Indicated are polar cap potential contours of the SuperDARN map-potential model and flow vectors based on SuperDARN measurements of the convection. Noon (12 MLT) is at the bottom of each panel.

Table 2a

N°	Class	Date	Start	Stop	# scans	Period [s]	Dur. [s]	Q	F.dir	abs(V_i)	M	W	Backg.	F.o.v.
1	S	16.01.2001	08:55	08:59	2	128	256	3	S/E	250-500			red	
2	S	16.01.2001	08:59	09:03	2	128	256	3	N/E	250-500			red	
3	S	16.01.2001	09:08	09:10	1	128	128	3	S/E	250-500			red	Poor data
4	S	16.01.2001	09:31	09:33	1	128	128	3	N/E	0-250			red	
1	E	16.01.2001	10:07	10:16	4	128	512	3	S/E	250-500			red	
5	S	16.01.2001	10:29	10:33	2	128	256	3	N/E	250-500			red	
6	S	16.01.2001	10:50	10:52	1	128	128	3	N/E	250-500			red	
7	S	17.01.2001	09:33	09:35	1	128	128	2	N/W	250-500			black	
8	S	19.01.2001	06:11	06:28	8	128	1024	1	S/W	250-500			black	
9	S	19.01.2001	10:27	10:29	1	128	128	2	S/E	0-250			black	
10	S	19.01.2001	10:31	10:33	1	128	128	2	S/E	0-250			black	
11	S	19.01.2001	10:35	10:39	2	128	256	2	S/E	0-250			red	
12	S	19.01.2001	11:18	11:22	2	128	256	2	S/E	0-250			red	
13	S	19.01.2001	11:35	11:41	3	128	384	2	S/E	250-500			red	
14	S	19.01.2001	11:43	11:46	1	128	128	2	S/E	250-500			red	
15	S	19.01.2001	11:54	11:56	1	128	128	2	S/E	0-250			red	
2	E	20.01.2001	06:45	06:49	2	128	256	1	S/W	250-500	N		red	
16	S	20.01.2001	10:01	10:05	2	128	256	2	S/E	250-500			red	
17	S	20.01.2001	10:22	10:27	2	128	256	2	S/E	250-500			red	
18	S	20.01.2001	10:22	10:27	2	128	256	2	S/E	0-250	S		red	
19	S	20.01.2001	10:29	10:31	1	128	128	2	S/E	0-250			red	
20	S	20.01.2001	10:31	10:37	3	128	384	2	S/E	0-250			red	
21	S	20.01.2001	10:44	10:48	2	128	256	2	S/E	0-250			red	
3	E	15.12.2001	07:36	07:43	2	192	384	1	N/E	250-500		x	blue	
22	S	15.12.2001	09:14	09:21	2	192	384	4	S/E	250-500			blue	
4	E	15.12.2001	09:24	09:27	1	192	192	1	N/E	250-500			blue	
23	S	15.12.2001	09:41	09:47	2	192	384	2	S/E	250-500			red	
5	E	15.12.2001	10:03	10:58	17	192	3264	2	S/E	250-500		x	red	X
6	E	16.12.2001	07:31	07:37	2	192	384	4	S/E	250-500			blue	
7	E	16.12.2001	08:03	08:52	15	192	2880	1	N/E	250-500			blue	
8	E	16.12.2001	08:39	08:48	3	192	576	1	N/E	250-500			blue	

Table 2 a) continued

N°	Class	Date	Start	Stop	# scans	Period	Dur. [s]	Q	F.dir	abs(V_i)	M	W	Backg.	F.o.v.
9	E	16.12.2001	08:52	09:30	12	192	2304	1	N/E	250-500		x	blue	X
10	E	16.12.2001	10:16	10:45	9	192	1728	3	N/E	250-500	N	x	red	
25	S	16.12.2001	10:29	10:35	2	192	384	2	S/E	250-500			red	
11	E	16.12.2001	10:51	10:59	3	192	576	3	N/E	250-500			red	X
26	S	17.12.2001	10:10	10:13	1	192	192	3	N/E	0-250			red	
27	S	17.12.2001	10:17	10:20	1	192	192	3	N/E	0-250			red	
12	E	18.12.2001	06:43	06:50	2	192	384	1	N/E	250-500			blue	
13	E	18.12.2001	07:54	08:03	3	192	576	1	N/E	250-500			blue	X
14	E	18.12.2001	09:38	10:07	9	192	1728	3	S/E	250-500	N	x	red	
15	E	18.12.2001	09:51	10:20	9	192	1728	3	S/E	250-500	N	x	red	
16	E	18.12.2001	10:07	10:30	7	192	1344	3	N/E	250-500	N	x	red	
28	S	19.12.2001	08:41	08:47	2	192	384	3	N/E	0-250			red	
17	E	20.12.2001	06:19	06:22	1	192	192	1	N/E	250-500			blue	
29	S	20.12.2001	06:51	06:57	2	192	384	1	N/E	250-500			blue	
30	S	20.12.2001	10:16	10:25	3	192	576	3	N/E	250-500			red	
18	E	20.12.2001	10:25	10:51	8	192	1536	3	S/E	250-500	N	x	red	
19	E	20.12.2001	10:41	10:57	5	192	960	3	N/E	250-500			red	X
20	E	21.12.2001	07:38	07:55	5	256	1280	3	S/W	250-500		x	blue	
21	E	21.12.2001	08:55	09:12	4	256	1024	3	S/W	250-500			blue	
31	S	21.12.2001	09:29	09:38	2	256	384	3	N/E	0-250			red	

2.3.4 Results from Table 2

The data set consists of roughly 36 hours of data, 767 scans in total. 21 RFEs spanning 123 scans have been identified, meaning that 16% of the scans contain RFEs. Moreover, 31 flow structures spanning 60 scans have been found, thus 7.8% of the scans contain these structures. If it is assumed that flow structures are caused by the same physical mechanisms as RFEs, but that they for some reason do not fully develop, it can be said that the total occurrence of flow channels is 23.9% of the observation time.

The MLT occurrence for the RFEs and flow structures is shown in Figur. Since the radar field-of-view extends over 2-4 hours in MLT depending on the current scan mode, it is not accurate to calculate the MLT dependence from the occurrence time in UT (+ 3

Table 2b

N°	Class	Date	Start	Stop	IMF B_z	IMF B_y	Certainty	SD coverage	SD match	Along/opposite F_t
1	S	16.01.2001	08:55	08:59	<0	>0	AA	Ok coverage	Ok match	opposite
2	S	16.01.2001	08:59	09:03	<0	>0	AA	Ok coverage	ok match	opposite
3	S	16.01.2001	09:08	09:10	<0	>0	AA	Ok coverage	ok match	opposite
4	S	16.01.2001	09:31	09:33	<0	<0	AC	Ok coverage	poor match	along
1	E	16.01.2001	10:07	10:16	**<0**	**<0**	AB	Ok coverage	No match	along
5	S	16.01.2001	10:29	10:33	<0	>0	AB	Ok coverage	Ok match	opposite
6	S	16.01.2001	10:50	10:52	<0	<0	AC	Ok coverage	Ok match	along
7	S	17.01.2001	09:33	09:35	>0	>0	AA	No data		along
8	S	19.01.2001	06:11	06:28	>0	>0	AB	Ok coverage	Ok match	along
9	S	19.01.2001	10:27	10:29	>0	>0	AA	Ok coverage	Ok match	opposite
10	S	19.01.2001	10:31	10:33	>0	>0	AA	Ok coverage	Ok match	opposite
11	S	19.01.2001	10:35	10:39	>0	>0	BA	Ok coverage	Ok match	opposite
12	S	19.01.2001	11:18	11:22	<0	>0	AA	Ok coverage	Ok match	opposite
13	S	19.01.2001	11:35	11:41	<0	>0	AA	Ok coverage	Ok match	opposite
14	S	19.01.2001	11:43	11:46	<0	>0	AA	Ok coverage	Ok match	opposite
15	S	19.01.2001	11:54	11:56	<0	>0	AA	Ok coverage	Ok match	opposite
2	E	20.01.2001	06:45	06:49	**<0**	**<0**	AA	Ok coverage	Ok match	opposite
16	S	20.01.2001	10:01	10:05	>0	>0	CA	No data		opposite
17	S	20.01.2001	10:22	10:27	>0	>0	AA	No data		opposite
18	S	20.01.2001	10:22	10:27	>0	>0	AA	No data		opposite
19	S	20.01.2001	10:29	10:31	>0	>0	AA	No data		opposite
20	S	20.01.2001	10:31	10:37	>0	>0	AA	No data		opposite
21	S	20.01.2001	10:44	10:48	>0	>0	AA	No data		opposite
3	E	15.12.2001	07:36	07:43	**fluct**	**>0**	CA	Poor coverage	Ok match	opposite
22	S	15.12.2001	09:14	09:21	fluct	>0	CA	Ok coverage	Ok match	opposite
4	E	15.12.2001	09:24	09:27	**fluct**	**>0**	BA	Ok coverage	Ok match	opposite
23	S	15.12.2001	09:41	09:47	>0	>0	BA	Ok coverage	Ok match	opposite
5	E	15.12.2001	10:03	10:58	**>0**	**>0**	CA	Ok coverage	Ok match	opposite
6	E	16.12.2001	07:31	07:37	**>0**	**>0**	AA	Ok coverage	Ok match	opposite
7	E	16.12.2001	08:03	08:52	**>0**	**>0**	AA	Ok coverage	Ok match	opposite
8	E	16.12.2001	08:39	08:48	**>0**	**>0**	AA	Ok coverage	Ok match	opposite
9	E	16.12.2001	08:52	09:30	**>0**	**>0**	AA	Ok coverage	No match	opposite
24	S	16.12.2001	09:44	09:50	>0	>0	AA	Ok coverage	Ok match	opposite

Table 2b continued

N°	Class	Date	Start	Stop	IMF B_z	IMF B_y	Certainty	SD coverage	SD match	Along/opposite F_t
10	E	16.12.2001	10:16	10:45	**>0**	**>0**	AA	Ok coverage	Ok match	opposite
25	S	16.12.2001	10:29	10:35	>0	>0	AA	Ok coverage	Ok match	opposite
11	E	16.12.2001	10:51	10:59	**>0**	**>0**	AA	Ok coverage	Ok match	opposite
26	S	17.12.2001	10:10	10:13	**>0**	**>0**	CA	Poor coverage	Poor match	opposite
27	S	17.12.2001	10:17	10:20	**>0**	**>0**	BA	Poor coverage	Poor match	opposite
12	E	18.12.2001	06:43	06:50	**<0**	**>0**	BA	No data		opposite
13	E	18.12.2001	07:54	08:03	**<0**	**>0**	BA	Ok coverage	Poor match	opposite
14	E	18.12.2001	09:38	10:07	**<0**	**>0**	AA	Ok coverage	Ok match	opposite
15	E	18.12.2001	09:51	10:20	**<0**	**>0**	AA	Ok coverage	Ok match	opposite
16	E	18.12.2001	10:07	10:30	**<0**	**>0**	AA	Ok coverage	Ok match	opposite
28	S	19.12.2001	08:41	08:47	**<0**	**>0**	AB	No data		opposite
17	E	20.12.2001	06:19	06:22	**<0**	**>0**	BA	Ok coverage	Poor match	opposite
29	S	20.12.2001	06:51	06:57	**>0**	**>0**	BA	Ok coverage	Ok match	opposite
30	S	20.12.2001	10:16	10:25	**<0**	**>0**	AA	Ok coverage	Ok match	opposite

hours to adjust for the magnetic longitude of Longyearbyen). If for example the radar is pointing west, an RFE will have an MLT extent of at least 2 hours in MLT in the radar field-of-view. Its start and stop times in UT refer to the easternmost position of the radar fan, located in Longyearbyen. A better estimate of the MLT occurrence was achieved by determining the mid-position in longitude of the radar fan and the MLT difference in minutes relative to Longyearbyen for every scan mode. The results are shown in column 10 of Table 1. The start and stop times of the RFEs and flow structures from Table 2 have then been adjusted according to the scan direction they where detected in to yield the start and stop times in the middle of the ESR fan.

As can be seen from Figur *a*, the occurrence of RFEs exhibits a clear maximum around 12 MLT with up to 8 RFEs observed, and the peak skewed slightly towards 13 MLT. The spikes seen in Figure 8 occur whenever RFEs overlapped for just one minute. The occurrence of structures in Figure 8*b* does not have a clear peak, but they are spread out between 10:30 and 14:30 MLT with 1-2 flow structures observed. Around 13 MLT, there are two thin peaks where three flow structures have occurred at the same time in MLT (but not simultaneously). The trend seen from Figure 8a is as well reflected in Figure 8*c* which shows the total occurrence of both RFEs and flow structures as a function of MLT.

However, it can be seen from Table 1 that not all hours between 6 and 12 UT have had the same data coverage. Hence, a relative occurrence plot for RFEs and flow structures has been generated and is shown in Figure 8a. In this figure the number of events at a certain MLT has been divided by the number of times the ESR has actually scanned that MLT. As for the occurrence of RFEs and structures, the time intervals with data coverage have been adjusted so that they reflect the middle of the radar scan for each mode. From Figure 7 *a* it can be seen that it has been scanned most frequently (more than five times) between 10:15 to 12:45 MLT. Figure 9b shows the relative occurrence of RFEs. The shape of the curve has not changed significantly from the one in Figure 8a except from the one RFE which occurred around 13:30 MLT during a period of low data coverage and has been weighted a lot. The shape of the curve for the relative occurrence of flow structures reflects the fact that flow structures which occurred during times of low data coverage have been weighted a lot.

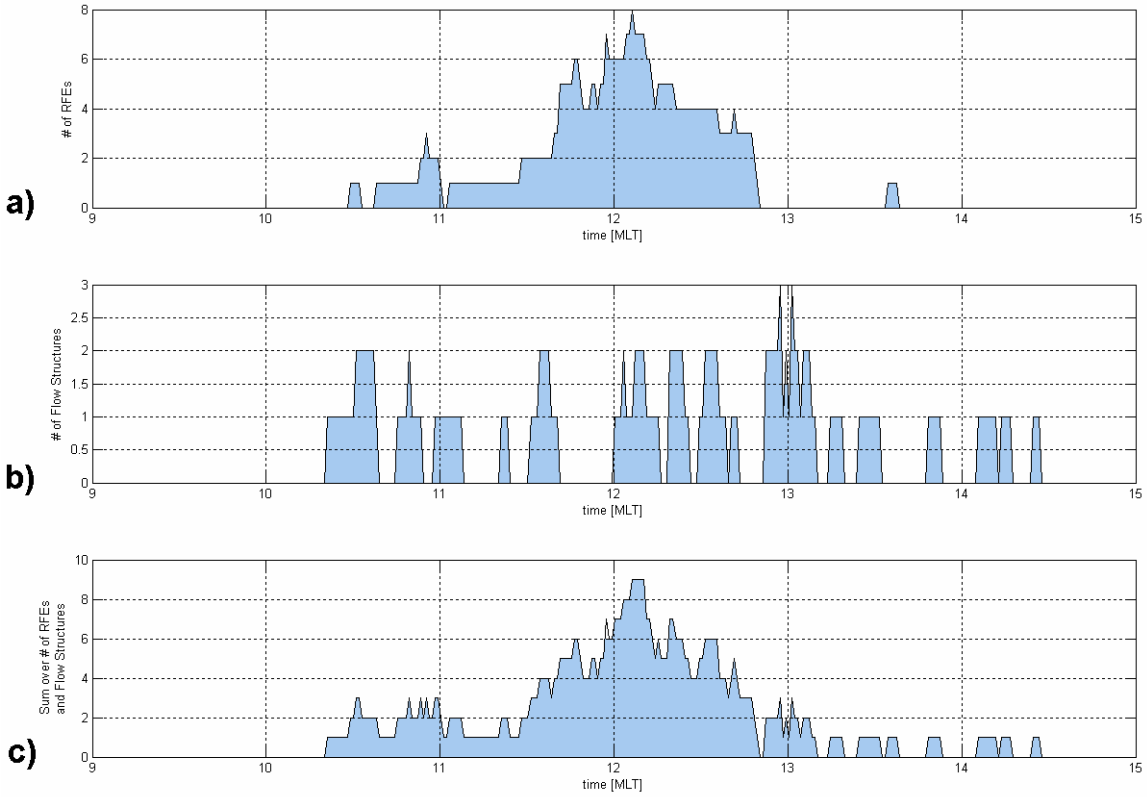

Figure 8 a) RFE b) Flow structure and c) total occurrence as a function of MLT. See text for details. The bin size is one minute.

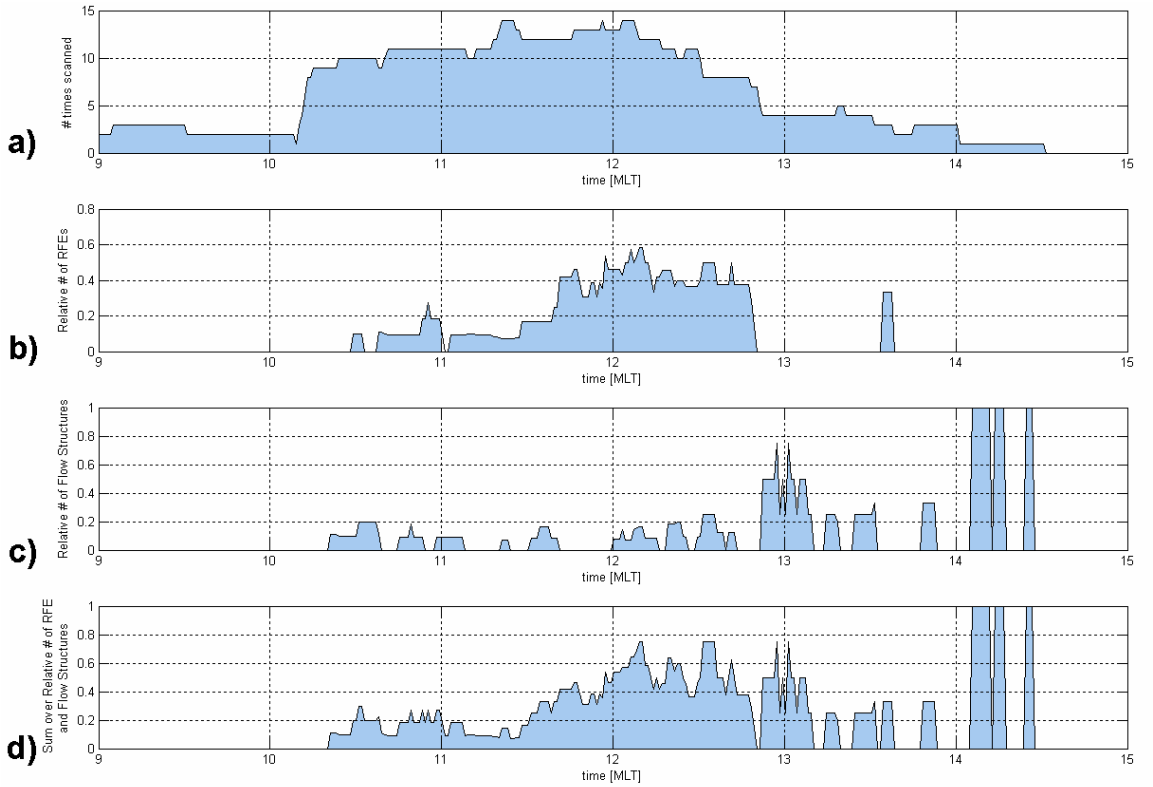

Figure 7: a) Data coverage as a function of MLT. The relative occurrence with respect to the data coverage of b) RFEs c) Flow structures and d) the sum of RFEs and flow structures as a function of MLT. See text for details. The bin size is 1 minute.

To get a relative estimate of how often RFEs and flow structures have occurred in a certain quadrant it is important to know how often each quadrant has been scanned. One radar sweep may extend over more than one quadrant. For example, 0-120° azimuth with 30° elevation scans the entire first quadrant and 33% of the fourth quadrant. This is accounted for by giving the first quadrant a count of 1.00 and the fourth quadrant a count of 0.33 for that radar sweep. For 360° azimuth, all four quadrants are visited during one radar sweep and each quadrant gets a count of 1.00. Using this method the total amount of single-quadrant scans is 1079.6. Of these 1079.6 scans, 35% (377.5 scans) was scanned in the first quadrant, 29.1% (314.8 scans) in the second, 23.8% (257 scans) in the third and 12.1% (130.3) in the fourth.

42.8% (9 RFEs) of all RFEs occurred in the first quadrant, 4.8% (1 RFE) in the second, 47.6% (10 RFEs) in the third and 4.8% (1 RFE) in the fourth quadrant. For flow structures the corresponding numbers are: 6.5% (2 flow structures) in the first quadrant, 51.6% (16 flow structures) in the second, 38.7% (12 flow structures) in the third, and 3.2% (1 flow structures) in the fourth.

If the number of scans in each quadrant is considered, the relative occurrence rate of RFEs is 10.9% of the time in the first quadrant (9 RFEs extending over 41 of 377.5 scans), 5.4% of the time in the second quadrant (1 RFE extending over 17 out of 314.8

scans), 24.5% of the time in the third quadrant (10 RFEs extending over 63 of 257 scans), and 1.5% of the time in the fourth quadrant (1 RFE extending over 2 of 130.3 scans). For the flow structures the relative occurrence rate is 2.6% of the time in the first quadrant (2 flow structures spanning 10 scans), 8.9% of the time in the second quadrant (16 flow structures spanning 28 scans), 7.8% of the time in the third quadrant (12 flow structures spanning 20 scans), and 1.5% of the time in the fourth quadrant (1 flow structure spanning 2 scans).

28.6% of the RFEs had southeast flow (6), 57.1% northeast (12) and 14.3% southwest flow (3). 58.1% of the flow structures had southeast flow (18), 35.5% northeast (11), 3.2% southwest (1) and 3.2% northwest (1)

The average duration of a RFE, calculated by multiplying the number of scans each RFE was observed with the scan period inferred from Table 1, was ~19 minutes. For flow structures the average duration was ~5 minutes.

In total, 5 RFEs (23.8%) were coincident with a change in the radar field-of-view, and only 1 flow structure (3.2%) occurred during an interval of poor data.

8 of the RFEs exhibit a behaviour as described in Figure 1. Four of them (RFE 10 with a lifetime of 1728 s, RFE 14 with a lifetime of 1728 s, RFE 15 with a lifetime of 1728 s, and RFE 18 with a lifetime of 1536 s) are seen from when they first form and until they fade or move out of the field-of-view. Their average lifetime was 28 minutes.

9 of the 21 RFEs in Table 2 exhibit a widening. Since 2 RFEs last for only one scan and cannot show any widening, this means that 9 of 19 RFEs (47.4%) were observed to broaden.

6 of 21 RFEs move northwards. Two RFEs are only visible in one single scan. Since motion cannot be determined for RFEs lasting only one scan, 6 of 19 RFEs have a northward motion (31.6%). Only one flow structure moved south during positive IMF B_y and B_z.

For the entire data set the IMF B_y component was negative only 8.7 % of the time, and the IMF B_z component was positive 42.8% of the time.

In total, 2 RFEs (9.5%) and 2 flow structures (6.5%) occurred during an interval of negative IMF B_y. 7 (33.3%) RFEs occurred during positive B_z, 4 (19%) RFEs were associated with "fluctuating" B_z. During all $B_z > 0$ or "fluctuating" B_z, B_y stayed positive. 17 (54.8%) structures occurred during B_z positive.

SuperDARN did not cover the location of the ESR field-of-view for 3 of 21 RFEs (14.2%) and 9 of 31 flow structures (29%). SuperDARN had OK coverage for 17 RFEs (81%) and 20 flow structures (64.5%) and poor coverage for 1 RFE (4.8%) and 2 flow structures (6.5%).

For 14 of 17 RFEs (82.4%) and 19 of 22 flow structures (86.4%) with SuperDARN coverage, the background convection observed by ESR was consistent with the flow of SuperDARN, and for 3 RFEs (17.6%) and 3 flow structures (13.6%) it did not match.

Of all 21 RFEs 18 (85.7%) exhibit ion flow in the direction opposite to what would be expected for the magnetic tension force for the given IMF. For flow structures 27 of 31 (87.1%) exhibit a flow opposite to the direction of the magnetic tension force.

If RFEs and flow structures without SuperDARN coverage are left out, 17 of 18 RFEs (94.4%) and 19 of 22 flow structures (86%) exhibit a flow in the direction opposite of the magnetic tension force. If in addition only RFEs and flow structures are included were SuperDARN has coverage and shows a consistent flow with the background inferred from the radar, 14 of 14 RFEs (100%) and 17 of 19 flow structures (89.5%) exhibit a flow in the opposite direction of the magnetic tension force.

2.3.5 Discussion

Since the amount of analyzed data (11 days spanning roughly 36 hours in 767 scans) is rather limited and may not be a fully representative selection of average conditions, the findings should be treated with some caution.

The findings of flow structures are not discussed separately here, since it remains to be proven whether or not they actually are related to RFEs. However, their existence indicates that flow disturbances are frequently occurring phenomena in the cusp, and the well-developed RFEs might just be the top of the iceberg.

Evaluating the total number of RFEs

Throughout the data set RFEs have occurred 16% of the time. There are several factors affecting this number:

1. The size and coverage of the ESR field-of-view compared to the size and location of the active cusp region at any given time
2. The geometry of observation and ability to observe RFEs

1. The size and coverage of the ESR field-of-view compared to the size and location of the active cusp region.

The cusp proper is a highly confined region, and there exists discordance about the extent in MLT of its footpoint in the ionosphere. Newell and Meng [1992; 2004] found the cusp to be 2.5 hours wide in MLT in their statistical study (see Figure 2.17). Maynard et al. [1997] however found the cusp to be at least 3.7 h in MLT in an event case study. The latitudinal extent of the cusp is only a few degrees or less. Newell and Meng [1988] found a latitudinal width of the cusp of ~1°, somewhat wider for positive IMF B_z than for negative B_z [Newell and Meng, 1987]. Newell and Meng [1988] studied the local time dependence of the cusp and showed that it is observed most frequently near 12 MLT. The latitudinal location of the cusp is believed to be between 70º N for IMF B_z south and 80º N for IMF B_z north, and mostly around 75º N for moderate conditions [Sandholt et al., 1998b].

The location of the cusp varies strongly with the orientation of the IMF. For a negative (positive) IMF B_y, the cusp shifts dawnward (duskward) [Cowley et al., 1991]. For a northward IMF B_z, the cusp remains more or less confined near noon at ~77-79° MLAT. For a southward IMF B_z, the cusp moves equatorward with more negative B_z. The IMF B_x component has no known effect on the cusp position [Newell et al., 1989].

Reconnection may however take place within LLBL and mantle in addition to the highly confined cusp proper. We therefore use the wide definition of the ionospheric cusp which includes LLBL, mantle and cusp. Depending on the solar wind pressure and IMF conditions, it is located somewhere between 9-15 MLT and 70-80º N, extending over 3-4 hours in MLT and a few degrees in latitude.

Scanning with a constant elevation of 30º the radar field-of-view extends over ~1.5 hours in MLT along the line-of-sight if pointed directly east or west, and ~7º in latitude if pointed north or south. The fan-shaped field-of-view spanned usually 90-120º in azimuth throughout the data set, which means that the radar field-of-view can see up to half the cusp.

2. The geometry of observation and ability to observe RFEs

In addition to the fact that the ESR field-of-view is only capable of seeing parts of the active cusp and that there are uncertainties with regard to the exact location of the cusp, the direction of plasma flow inside a RFE as well as the large-scale convection in the polar cap is important for whether or not the radar is sensitive to flow events. The radar is only sensitive to plasma motion along its line-of-sight, and insensitive to plasma flow perpendicular to the pointing direction. According to point *iv)* of the RFE definition, the RFE has to stay in clear contrast with the background. This means that the background flow must exhibit uniform velocity higher than ±|250| m/s along the line-of-sight in the region of the RFE and so must the RFE itself. Hence, RFEs cannot be detected when either large-scale background convection and/or the RFE flow channel is directed perpendicular to the radar line-of-sight.

Assume an ion flow velocity of ~1000 m/s, the ±|250| m/s criterion means a maximum angle between the flow vector and ESR line-of-sight of 75°. Any larger offset will result in an ion flow component along the ESR line-of sight smaller than |250| m/s and hence not qualify for RFE detection.

<u>Evaluating the MLT occurrence of RFEs</u>

The MLT occurrence plot for RFEs in Figure 8*a* revealed that the maximum occurrence of RFEs was around 12 MLT but skewed slightly over towards the post-noon sector. The activity peaked with the total number of 8 RFEs around 12:15 MLT. No activity occurred before 10:30 MLT and activity was low with in average 1 RFE occurring between 10:30 and 11:30 MLT before it tripled from 2 to 6 RFEs just after 11:30 MLT. The RFE activity was high with 4 to 8 RFEs between 11:45 and 12:45 MLT before a steep decrease to zero just prior to 13 MLT. One event occurred around 13:30 MLT. Since the IMF B_y was predominantly positive in the available data set, the apparent post-noon shift of the activity occurrence is consistent with RFEs being cusp related phenomena, as the active cusp is expected to be shifted over towards post-noon for positive B_y.

However, our data base does not represent a uniform MLT coverage between 9-15 MLT. Figure 7 *a* reveals that the radar scanned the region between 10:15 and 12:45 MLT more than five times (mostly around 10 times) whereas the regions between 09:00 and 10:15 MLT, and 12:45 and 14:30 MLT were scanned less than five times. Between 12:45 and 14:00 MLT the radar scanned mostly around 3 to 4 times, whereas the other region with low data coverage has been scanned less than 3 times. The relative occurrence of RFE is shown in Figure 7 *b*.

The RFE activity onset occurred at 10:30 MLT and was low between 10:30 and ~11:45 MLT. One single RFE occurred during an interval of low data coverage post-noon. The size of its peak has been given full weight when calculating the relative occurrence since it occurred during a time with poor data coverage. Not much importance should be paid to the size of such a single-event peak. At 11:45 MLT, the activity increased steeply and remained high until a steep decrease at ~12:45 MLT. Comparing Figure 9 *a* and Figure 9 *b*, the increase of activity pre-noon occurred in a region with high data coverage, but the steep decrease of event occurrence in the post-noon sector coincides with a steep decrease in data coverage. Hence, the distribution of the event occurrence may be strongly affected by the MLT coverage on the post-noon side. For a predominantly positive IMF B_y a peak slightly post-noon as seen in Figure 7 *b* would fit well with RFE being a cusp phenomenon. How far post-noon activity extends is however difficult to say do to the drop in data coverage. Placing the RFEs in the context of SuperDARN polar cap convection patterns shows that RFEs are predominantly located in regions of enhanced plasma flow at the border of the inflow region of the afternoon cell. However, larger amounts of data and case studies, which may link RFEs to auroral activity and thereby prove the assumption, should be analyzed.

Evaluating the appearance rate per quadrant and the ion flow direction

Of the time scanned in each quadrant, events occurred much more frequently in the first and third quadrant (Q1 and Q3) than in the second an fourth (Q2 and Q4), and more than twice as often in the third than in the first quadrant. In the context of SuperDARN large-scale convection maps the RFEs were located in regions of enhanced plasma convection close to or within the cusp inflow region. Furthermore, from the IMF plots it became clear that all events did have a nonzero IMF B_y component and in the majority of the RFEs, IMF B_y was >3 nT consistent with a large zonal flow component. During moderate activity the auroral oval is centred on 75° MLAT, i.e. close to Longyearbyen. Due to the dipole tilt, the auroral oval will then span quadrants Q1 and Q3 of Figure 3. Q4 will be covered by aurora in the case of an expanded polar cap. Similarly, the cusp may be situated in Q2 when polar cap is contracted. The ESR is only sensitive to plasma flow along its line-of-sight. In cases where the zonal flow component along the auroral oval dominates (large IMF B_y) ESR will be most sensitive to RFEs in sectors Q1 and Q3 of Figure 3. RFEs in Q2 and Q4 can be detected by ESR only when there is a strong meridional flow component, i.e. when IMF B_y is weak.

Most of the scans from Q2 were scanned during January 2001 and did not qualify very well for event detection due to speckle or a low velocity background. In general, data

collected in January 2001 was more speckled and non-uniform than data from the December 2001 runs, and the background velocity was low during a larger number of January scans than in December. This is also reflected in Table 2. Only 2 of the 21 RFEs, but 21 of 31 flow signatures occurred in January. From the RFE criteria, the background must be uniform and have high velocity in order to qualify for RFE detection. The most likely reason for the discrepancy between January and December scans is that the computer network at the radar site was upgraded during the summer of 2001. In January 2001 the computer network had severe problems to keep up with the high flow of data, and occasionally data sequences were lost and not saved to disk. At times 10% of the data was lost. There were also more problems with the air traffic warning system. In periods it shut off the transmission over and over again and had to be manually reset. Examining the occurrence of flow structures, it becomes apparent that flow structures actually occurred most frequently in Q2. Thus, it seems as if the reason for the low appearance of RFEs in Q2 may be partly related to data quality, but also to the fact that ESR is not sensitive to Q2 for a nonzero IMF B_y as discussed above. The poorer data quality during January can also explain why RFEs occurred more frequently in Q1 than in Q3 since Q1 was mainly scanned in January, whereas Q3 was scanned mostly in December.

Factors that influence the lifetime of RFEs

Almost every fourth RFE was determined by a change in the radar field-of-view. This obviously influences the average lifetime calculated. Four very prominent RFEs were found to develop from a small-scale reduction of background flow into a large RFE (like the one shown in Figure 1). The background flow in the ESR field-of-view was very uniform during all these RFEs. Their lifetime was 28 minutes and hence ~10 minutes longer than the average lifetime of 19 minutes. From a study like the one presented here, it is not possible to further parameterize the lifetime.

Widening and motion of RFEs

Almost one half of the RFEs widened during their lifetime. Why they widen is not known. Around 30% of the RFEs move north. Motion and widening does not seem to be connected, since not all events that widen move, and not all that move widen. Further studies are needed.

IMF dependence

The IMF B_z component was negative 57.2% of the time, and 66.7% of the RFEs occurred during an interval of positive B_z. It seems thus as if the occurrence is independent of IMF B_z. 91.3% of the time the IMF B_y component was positive and 90.5% of the RFEs occurred during positive B_y conditions. For IMF B_y, the number of scans and events involved is really too low to judge the B_y polarity dependence in RFEs. However the occurrence of RFEs is not exclusive related to one polarity if IMF B_y.

Possible explanation of the RFE signatures

The MLT occurrence and the location of RFEs with respect to the large-scale polar cap convection monitored by SuperDARN indicate that RFEs are a phenomenon occurring near the active cusp. It is therefore natural to consider RFEs a possible signature of reconnection events.

According to the theory presented by Southwood [1985; 1987], hereafter referred to as the Southwood model, the ionospheric signature of an FTE is proposed to be a mesoscale twin-cell flow disturbance. This twin-cell pattern is understood as newly opened flux pushing its way through the plasma and thereby creating return flow on either side. Lockwood et al. [1990b] pointed out that the Southwood model is based on the concept that a newly opened flux tube moves faster than the surrounding plasma since no return flow could arise if they would move at the speed of the background plasma. As soon as the flux tube has unbent, however, it behaves like any other background tube and can no longer overtake surrounding tubes, and the vortex flow pattern disappears. Lockwood et al. [1990a] showed that the production of newly opened flux at the dayside magnetopause excites magnetospheric and ionospheric flows only for a short interval of ~10 minutes. Subsequently, any flows driven by this source decay on this time scale unless they are maintained by further production of newly opened flux. He thus estimated the lifetime of Southwood [1985; 1987] FTE twin vortex flow to roughly ~10 minutes. Furthermore, Lockwood et al. [1990b] suggested that the return flow in the Southwood model may not be very pronounced. According to Lockwood et al. [1990b], newly opened flux tubes in the ionosphere are typically 250 km in north-south extent and 1500-2000 km in east-west extent.

Pinnock et al. [1993] reported the observation of an enhanced convection channel (ECC) in the cusp ionosphere. Combined observations by the PACE (Polar Anglo-American Conjugate Experiment) HF radar and the DMSP F9 polar-orbiting satellite revealed a "longitudinally elongated (>900 km), latitudinally narrow (~100 km) channel of enhanced convection". Within the channel, which had a flow direction in the same direction as the background flow, the line-of-sight velocity was enhanced compared to the background flow, and in the regions bordering the channel, the background flow was somewhat slower. Pinnock et al. [1993] interpreted this as evidence for weak return flow outside the convection channel. Since the return flow opposed the background flow with much larger velocity, the net effect was a reduction rather than a return flow, in accordance with Lockwood et al. [1990b].

Marchaudon et al. [2004] observed an azimuthally elongated convection enhancement by two SuperDARN radars in conjunction with FACs observed by the Ørsted satellite. They found that the direction of the FAC pair was in agreement with the Southwood model and that current density of each FAC and the Pedersen current densities indicated that the closure current for this FACs pair occurred inside the flow burst. The dimensions of the ionospheric convection enhancement where 100×1000 km and the flow inside the channel was larger than 1000 m/s and exceeded the background flow. They claim the validity of the Southwood model based on their observations.

Oksavik et al. [2004; 2005] reported the signature of a twin-cell pattern in association with a PMAF observed by a conjunct of the ESR and an all-sky camera in the present data set and interpreted it as the signature of an FTE according to the Southwood model. The enhanced convection channel interpreted as the centre flux in the Southwood model was only 50-60 km wide, and surrounded by flow running in the opposite direction. The

PMAF was situated at the poleward edge of the flow channel thereby being consistent with the signature of an upward going Birkeland current filament as predicted by the Southwood model.

All reported flow disturbances listed above were interpreted as ionospheric signatures of Southwood [1985; 1987] FTE model. Denig et al. [1993] observed as well indications of an FTE twin-cell by DMSP and Sandholt et al. [1990] reported indications of an FTE twin cell travelling across the EISCAT UHF beam pointing north from Tromsø. Oksavik et al. [2004] provides the only example where the spatial structure of a meso-scale twin-cell system has been mapped out by direct measurements.

The ion flow direction of RFEs was defined to be in the opposite direction of the background flow observed in the ESR field-of-view. Furthermore, in 85.7% of the time, the RFE flow direction was opposite to the direction of the magnetic tension force suggested by IMF condition. In general, SuperDARN gave good coverage and confirmed the background flow seen by the ESR radar. If RFEs without SuperDARN coverage are left out, 94.4% of the RFEs have a flow opposite to the direction of the magnetic tension force. If RFEs during intervals when the SuperDARN background flow did not match the ESR background flow are excluded too, 14 of 14 RFEs (100%) exhibit an ion flow opposite to the magnetic tension force. Hence, RFEs can definitely not be interpreted in terms of the centre flux and FTE twin-vortex flow pattern for two reasons: Their flow is opposite to the background flow, and their motion is opposite to the IMF B_y controlled magnetic tension force pull on newly opened field lines.

If RFEs are related to the Southwood FTE model, they correspond to the return flow; as suggested by Oksavik et al. [2004]. Moreover, from the RFE definition they have to extend over at least 400-600 km in the ESR field-of-view. No RFE was found in the data set where the longitudinal extent did not exceed the ESR field-of-view. Hence, it seems as if RFEs exceed 600 km in length. Since the longitudinal dimension of the return flow would have to be approximately equal to the longitudinal extent of the centre flux, the spatial dimensions appear consistent with the dimension suggested by Lockwood et al. [1990b].

The Southwood model predicts two return flow channels on the equatorward and poleward edge of the centre flux respectively. Throughout the entire data set, there were only three occasions in which two RFEs coexisted within the ESR field-of-view. Since these occasions where similar, only one of them which was presented by Oksavik et al. [2004; 2005] is shown in Figure 8. Oksavik et al. [2004; 2005] presented the scans which are framed, number 7, 9 and 11 in Figure 8. They observed the signature of a Southwood twin-vortex flow, where the narrow region of enhanced ion flow directed away from the radar indicated by the red arrow in the ninth scan from 10:04-10:07 UT was classified as the signature of the centre flux in the Southwood model, and the areas of flow directed towards the radar termed “14” and “15” as the return flow predicted by the Southwood model. The direction of the centre flux as defined by Oksavik et al. [2004; 2005] is consistent with the background flow inferred from SuperDARN convection maps and the direction of the magnetic tension force for the given IMF conditions. In this thesis, the

RFE onset was defined as the first sign of reduction in the background flow which later developed to a prominent RFE. From 09:23 UT onwards the ESR scanned the region shown in Figure 8. The background flow in the radar field-of-view was uniform and directed away from the radar with some reduced/reversed flow in the southern part of the scan since the region discussed here was scanned. This background flow matched the flow indicated by SuperDARN. At 09:38 UT, which is defined as the onset of event 14 in Table 2, a region of reversed flow became visible, marked out by the yellow ellipse in the top left panel of Figure 8. This flow signature grows in size and develops into a large and strong RFE at 9:48 UT in the fourth scan. Some minutes later, at 9:51 UT, a second region of reversed flow is indicated by the yellow arrow in panel 5. It rapidly develops into a RFE which is listed as number 15 in Table 2. Both RFEs coexist and are termed "14" and "15" from the third and seventh scan onwards in Figure 8. RFE 14 moves out of the field-of-view after 10:07 UT.

Thus, following the criteria applied in this thesis, even though two RFEs coexist inside the ESR field-of-view from 9:51-10:07 Ut (scans 5-9), they did not occur simultaneously, but with a delay of ~13 minutes. According to the Southwood FTE model, the return flow from a newly reconnected field line moving through the ionosphere is expected to occur simultaneously, and hence the two RFEs cannot be regarded as the return flow channels surrounding one single event of newly opened flux, but have to be regarded as separate flow events. Throughout the data set, there are only three cases where 2 RFEs coexisted within the ESR field-of-view. In the other two cases which are not presented here, there was a time delay between onset of ~36 and ~17 minutes.

So far we have documented reversed flow events. If these are signatures of the return flow in the Southwood model their onset must be a result of a magnetic tension pull of newly opened flux. In the case of IMF $B_y > 0$ (<0) the event onset should be seen as a region of strongly enhanced westward (eastward) flow, in-between two regions of reversed flow. Since the ESR does not observe two simultaneous return flow channels as predicted by the Southwood FTE model within its field-of-view it is difficult to determine which of the two return channels is represented by the RFE. Hence, from the ESR observations alone it cannot be determined for sure on which side of the RFE the flow enhancement associated with the motion of the newly reconnected flux tube it is located. However, Oksavik et al. [2004] found a PMAF coinciding with the equatorward edge of RFE 14. The location of this PMAF indicates that a upward going Birkeland current has to be located at the equatorward edge of RFE 14, and hence it can be identified as the poleward of the two return flow channels (see Figure 9 *a*). At the same time as RFE 14 develops from a flow structure to a RFE in the ESR field-of-view over the first four scans of Figure 8, a region of strong, westward convection becomes visible at its equatorward side, consistent with the expected direction of motion of newly reconnected flux. Hence, RFE 14 and the red region of enhanced westward flow equatorward of it may be a signature of the poleward clockwise cell of a Southwood FTE. Weak signs of return flow from RFE 14 may be visible at the equatorward edge of the first four scans, but this may as well be an effect of a general poleward drift of the background. RFE 15 develops ~13 minutes after RFE 14 and is as well associated with a belt of strong westward convection equatorward of it, best visible in the 9th and 10th scans

of Figure 8. Due to its non-simultaneous occurrence with respect to RFE 14, RFE 15 has to be regarded as the poleward return flux of a second FTE. This is in disagreement with Oksavik et al. [2004]. They interpreted RFE 14 and RFE 15 as the return flow of the same FTE event.

The EISCAT field-of-view should be large enough to observe the equatorward return flow if so exists. Oksavik et al. [2004] claimed they did. One may therefore ask why only one flow cell or 2/3 of a Southwood flow disturbance is observed throughout the data set. This question will have to be remained unanswered until further case studies reveal more details. There is one obvious difference between the two return flow regions of Southwood FTE. While the return flow poleward of the newly opened flux is on open field lines, the return flow equatorward of the newly open flux has to be on closed field lines. This is indicated in Figure 9 *a* by the grey line marked "OCB". The suggestion will however have to be proven by determining the precise location of the OCB by satellite measurements.

As mentioned above, Lockwood et al. [1990b] argued that the return flow in the Southwood model may not be very pronounced. An amplification effect of the poleward return flow in Southwood FTE model has however been suggested by Skjæveland [2005]. In the case of the winter polar cap, the background ionospheric conductivity will be low. Therefore, a significant accumulation of negative charges may occur underneath the upward going Birkeland current situated at the poleward edge of the newly reconnected flux tube. This accumulation is indicated by the grey shaded region in Figure 9 *a* and identified as the signature of an PMAF equatorwards of RFE 14 by Oksavik et al. [2004]. Hence, one electric field would arise and point across the flux tube towards the electron accumulation from the south (as indicated by black *E*-field vectors Figure 9 *b*), and a second electric field would point towards the electron accumulation from the north, indicated by the grey *E*- field arrows in Figure 9 *b*. The $E \times B$ drifts arising from these two *E*-fields are indicated by "$E \times B$" and enhance the motion of the newly reconnected field line and the poleward return flow respectively. Thus, the clockwise cell flow of the Southwood FTE model may be associated with a polarization electric field. Whether or not such a polarization effect can be large enough to accelerate the return flow is not known.

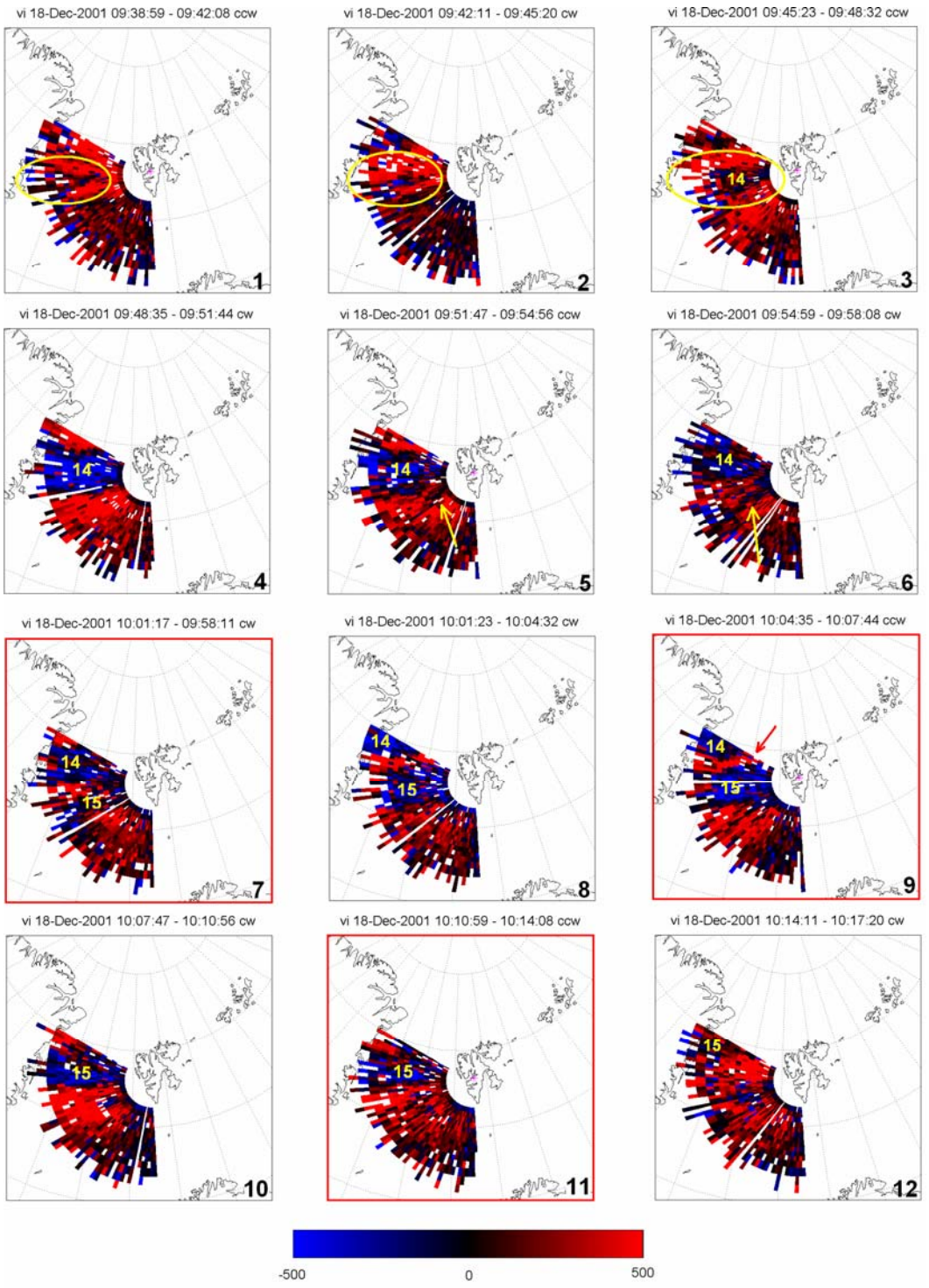

Figure 8: Ion velocity plot from 18.12.2001, covering RFE 14 and 15 in table 5.2. The scans presented by Oksavik et al. [2004] are framed red. The first signs of RFE 14 as interpreted in this thesis are encircled by a yellow ellipse; the first signs of RFE 15 are indicated by a yellow arrow. Numbers "14" and "15" indicate RFE 14 and 15 which have been interpreted as Southwood [1987] return flow by Oksavik et al. [2004]. The red arrow indicates the Southwood centre flow as interpreted by Oksavik et al. [2004].

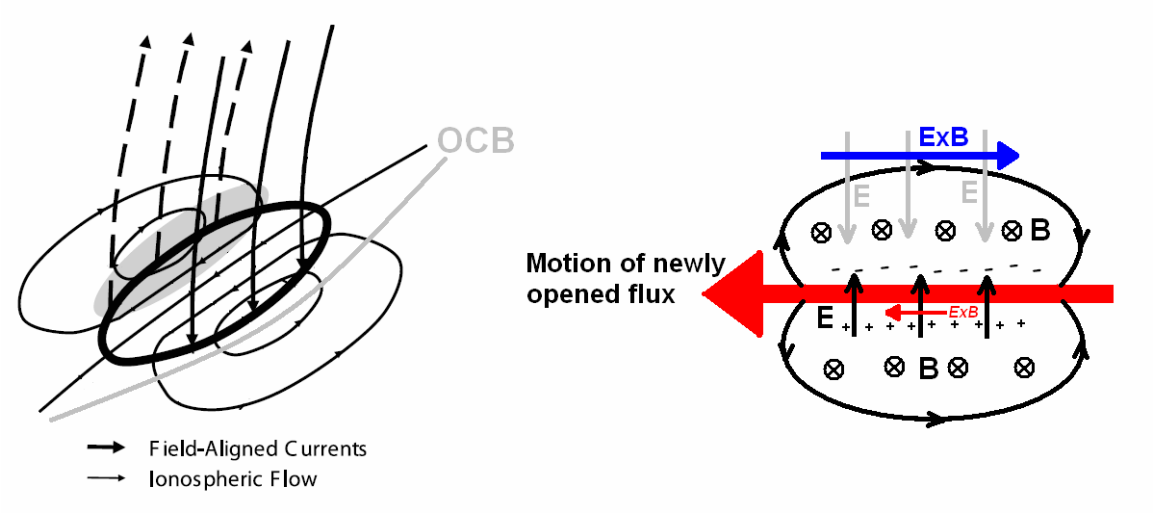

Figure 9:a) Schematic illustration of the Southwood model. The black ellipse is the foot point of a newly reconnected flux tube moving towards the left. On its side, downward and upward Birkeland currents are visible, and the twin-cell return flow is indicated. The grey shaded area indicates the region where electrons precipitate. b) Southwood model seen from above. The red arrow indicates the motion of the footpoint of the newly opened field line. The black curved arrows indicate the return flow. E and B fields are indicated as well. The upward and downward going Birkeland currents on the side of the flux tubes are indicated by "-" and "+", respectively. The blue arrow marked with "E×B" indicates enhanced return convection flow.

2.3.6 Summary and concluding remarks

From the discussion above it can be concluded that RFEs seem to be a regular feature of the cusp, occurring at least 16% of the time in the current data set. Since there are several constraints like the cusp location and the limited radar field-of-view, the line of sight viewing geometry with respect to the flow pattern and a strict RFE definition, it is likely that the occurrence rate is considerably larger. RFEs occurred near the cusp inflow region in the MLT range from ~11:45 to 12:45 MLT. They occurred in association with enhanced large-scale plasma flow observed by SuperDARN and seemed to be aligned with the auroral oval (L-shell aligned). The average lifetime of RFEs was 19 minutes. However, their lifetime can be even longer, since ~25% of the events were interrupted by a change of the radar field-of-view. No general motion or widening could be found. Furthermore, RFEs seem to occur independently of the IMF B_y and B_z polarity. The data set is strongly biased towards IMF B_y positive (IMF B_y was positive for ~91% of the events). The fact that 9.5% of the RFEs occurred during IMF B_y negative, however, indicates that the phenomenon is not exclusively related to one B_y polarity.

More than 85% of the RFEs detected in the data set had an ion flow opposite to the magnetic tension force. Hence, they cannot directly be interpreted as ionospheric signatures of newly opened flux, but there exists strong evidence that they can be interpreted as return flow in the Southwood model. RFEs do however not occur in pairs, and further studies will have to reveal why only the 2/3 of a Southwood twin cell pattern (on open flux) is visible and the return flow (on closed flux) is not.

3. Key Personell:

Prof. Jøran Moen (UiO)
Prof. Alv Egeland (UiO)
Prof. Jan. A. Holtet (UiO)
Dr. Kjellmar Oksavik (UiO)
Dr. Dag Lorentzen (UNIS)
Dr. Bjørn Lybekk (UiO)
Mr. Bjørn-Tore Esjeholm (UiO/HiF)
Ms. Yvonne Rinne (UiO)
and graduate students.